Exploring the Single-Electron Regime of a Double Quantum Dot in the Circuit Quantum Electrodynamics Architecture

J. Basset,[1] D.-D. Jarausch,[1] A. Stockklauser,[1] T. Frey,[1] C. Reichl,[1]
W. Wegscheider,[1] T. M. Ihn,[1] K. Ensslin,[1] and A. Wallraff[1]

[1]*Department of Physics, ETH Zurich, CH-8093 Zurich, Switzerland*

We have realized a hybrid solid-state quantum device in which a single-electron semiconductor double quantum dot dipole couples to the voltage oscillations of a nearby superconducting transmission line resonator. The amplitude and phase of the microwave tone transmitted through the resonator allow for determining the coherence properties of the double dot and measuring its interdot tunnel coupling. The value and uncertainty of the tunnel coupling was determined both with the microwave read-out technique and a standard quantum point contact charge detector. We demonstrate that the two techniques are equivalent with a superior precision for the microwave experiment. Decoherence properties of the dots, compared within the same sample in the single-electron and many-electron regimes, are also found equivalent.

PACS numbers: 73.21.La, 03.67.Lx, 42.50.Pq, 73.63.Kv

Circuit quantum electrodynamics and semiconductor nanophysics are closely related to each other and have prospered independently for more than a decade [1–9]. Only very recently a number of experimental efforts have been put forward to combine the physics of the two fields following theoretical proposals suggesting the advantages of this combination [10–15]. So far the hybrid architecture, consisting of quantum dots and a superconducting resonator, was successfully used to study many-electron devices [16–21]. In each of these experiments, one element was used to study the properties of the other i.e. the resonator response allowed to probe the properties of the dot system [16–21] or vice-versa [22]. However, an important milestone remaining to be reached is the strong coupling regime of cavity QED in which an entangled state between the resonator and the dot is formed [23]. To reach this regime is very demanding with quantum dots due to the poor control over the decoherence mechanisms that limit charge relaxation and dephasing rates. A suspicion that has been put forward by previous work [17, 19] is that excited states that are close in energy might enhance the energy relaxation (≈ 100 MHz) and the dephasing rate ($1-3$ GHz) of the qubit. As a result, decoherence rates are larger than the coupling rate (≈ 50 MHz) to the resonator. Therefore, the strong coupling limit has not yet been reached.

In this work we demonstrate that a superconducting resonator coupled to a double quantum dot is an exquisite sensor of the dot polarizability. In particular we show that such a system allows to determine tunneling properties of the double dot system with higher precision than a typical charge detection scheme using a quantum point contact. The uncertainty in our system is reduced by a factor of 1 to 20 compared to the quantum point contact. We further use the resonator to probe the quantum coherence properties of the double dot depending on the number of electrons residing in the dots. To do so we have fabricated a device in which the number of electrons can be controlled down to the last electron. An analysis comparing, within the same sample, a single-electron *vs* a many-electron (≈ 50 electrons in each dot) double dot shows that excited states play a minor role in the decoherence rate of our system.

The sample consists of a 200 nm thick superconducting coplanar waveguide resonator made of aluminum and patterned on top of a GaAs substrate, see Ref. [17, 18]. The coupling to the external microwave feed lines is realized through finger capacitors realizing an over-coupled resonator. The resonance frequency and loaded quality factor obtained with this geometry were $\nu_0 = 6.76$ GHz

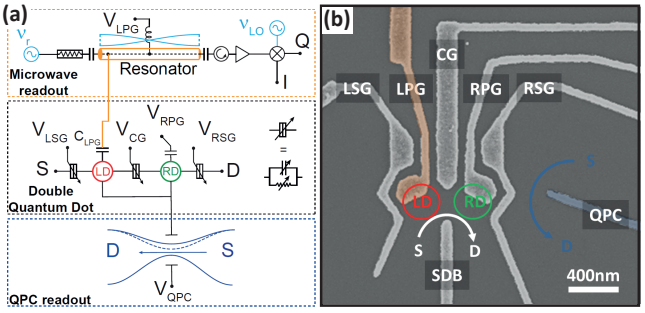

FIG. 1: (a) Circuit diagram representation of the double quantum dot (center panel) coupled to the resonator (top panel) and the quantum point contact (bottom panel). The double quantum dot is tuned with gate voltages V_{LPG}, V_{RPG}, V_{CG}, V_{SDB}, V_{LSG}, V_{RSG}. It is connected to the resonator via the capacitance C_{LPG}. The resonator is driven with a microwave signal at frequency ν_{r}. The transmitted signal passes through a circulator, is amplified and mixed with the local oscillator ν_{LO} to obtain the field quadratures I and Q. The quantum point contact is tuned with voltage V_{QPC}. (b) Scanning electron microscope picture of a double quantum dot gate design similar to the one used in the experiment. The gate extending from the resonator is colored in orange. The gate QPC used for charge detection is colored in blue.

and $Q \approx 920$ respectively corresponding to a decay rate of the resonator $\kappa/2\pi \approx 7.3$ MHz. A gate of small dimension compared to the resonator length is connected to the left hand side of the center conductor of the resonator where its first eigenmode has a maximum of the electric field (see top panel of Fig. 1a). This gate is directed towards a region where a two-dimensional electron gas (2DEG) is buried 90 nm below the surface. We fabricate in the middle of this 2DEG region (see Fig. 1b and center panel of Fig. 1a) a split-gate device by electron-beam lithography allowing for the formation of a double dot. The coupling between the double quantum dot and the resonator is mediated by the left plunger gate (LPG) extending from the resonator (orange colored gate) which selectively addresses the left quantum dot. The large size of the plunger gates was used to increase the dipolar coupling compared to standard designs used in the literature [4, 24, 26]. This modified design contains two major changes with respect to hybrid architectures so far realized in 2DEGs [17, 20]. First, the mesa edge is not part of the confining potential and second, an additional quantum point contact is fabricated on the right hand side of the double dot (blue colored gate QPC in Fig. 1b). These two changes allow for tuning the double-dot into a regime where a single electron is shared between the two dots [2, 28] as discussed further below. This sample is then mounted on a printed circuit board to which both microwave and dc connectors are attached. The board is assembled into a Copper box thermally anchored to the cold plate of a pulse-tube dilution refrigerator at a base temperature of approximately 10 mK.

By applying suitable negative voltages to all gates presented in Fig. 1b, we formed a double quantum dot potential and recorded the current flowing through the structure from source (S) to drain (D). When we tune the dot to the last electron, negative plunger gate voltages unselectively pinch-off the coupling to the reservoirs. We therefore use the nearby quantum point contact (QPC colored in blue in Fig. 1b) as a charge sensor [27, 28]. Recording the transconductance $dI_{\mathrm{CD}}/dV_{\mathrm{LPG}}$ versus LPG-RPG gate voltages using a standard lock-in technique, we observe the hexagon-shaped charge stability diagram of the double quantum dot (see Fig. 2a) [28]. The absence of resonances in the bottom left corner of Fig. 2a indicates that the double dot is completely depleted [28]. Starting from this region, we assign the absolute number of electrons (M, N) in each of the dots and identify the $(0,1) \leftrightarrow (1,0)$ transition of interest here.

We measure the dot using the resonator by applying a coherent microwave signal at frequency ν_0 to the resonator and extract the amplitude A and phase ϕ of the transmitted signal from the measured field quadratures I and Q, as $Ae^{i\phi} = I + iQ$ in a heterodyne detection scheme (see top panel of Fig. 1a) [3]. Figure 2b shows that only the transition $(0,1) \leftrightarrow (1,0)$ influences the transmission amplitude. In particular, for the set of

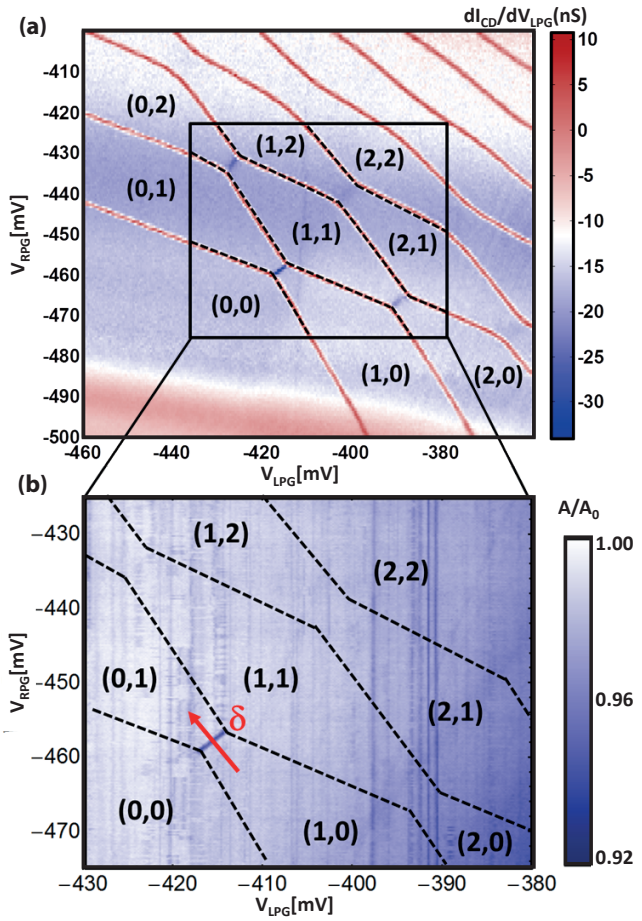

FIG. 2: (a) Colormap of the transconductance $dI_{\mathrm{CD}}/dV_{\mathrm{LPG}}$ as a function of V_{LPG} and V_{RPG} obtained with the QPC as a charge detector. (b) Normalized transmitted amplitude through the resonator as a function of V_{LPG} and V_{RPG} in the range indicated in (a). In each case, black dashed lines highlight boundaries between different charge states extracted from the measurement shown in (a).

parameters chosen here, the resonator signal exhibits a dip in amplitude. This observation has to be contrasted with previous equivalent experiments conducted in the many-electron regime [17, 18, 20], where charge degeneracy lines were observed over a large range of electron numbers in the dots. This is due to two properties of the present device: first, the plunger gates have a strong influence on the tunneling between the dots and second, the resonator is only sensitive to the charge delocalization in a very limited range of tunnel coupling t on the order of the resonator frequency ν_0 as emphasized later on. We have verified that making use of different gate voltage configurations allowed for the observation of other charge-degeneracy lines such as the $(1,1) \leftrightarrow (2,0)|(0,2)$ and so on. However, in the many-electron regime we recover the results of Ref. 17.

We now focus on the $(0,1) \leftrightarrow (1,0)$ charge-degeneracy

line which we systematically study as a function of the tunnel coupling t between the dots. In a first set of measurements, we analyze the QPC response and extract from it the tunneling amplitude when an electron is delocalized between the dots [29]. In a second step, we extract t from the resonator response [17]. We finally compare the values for t and its uncertainty obtained using the two techniques.

When tuning across the charge degeneracy line δ shown by a red arrow in Fig. 2b, the electron distribution is shifted from the left dot to the right dot. This change in charge distribution leads to changes in the effective saddle point potential of the right QPC, reducing its conductance. Measuring this change as a function of detuning δ allows us to determine the average occupation of the left dot which continuously varies from 1 to 0. The shape of this average charge occupation number $\langle m \rangle$ depends on the tunnel coupling t between the dots and on the electronic temperature T_e [29]:

$$\langle m \rangle = \frac{1}{2}\left[1 - \frac{\delta}{\sqrt{\delta^2 + (2t)^2}} \tanh\left(\frac{\sqrt{\delta^2 + (2t)^2}}{2k_B T_e}\right)\right]. \quad (1)$$

We determine the electron temperature $T_e = 130$ mK from independent Coulomb blockade diamond measurements of a single dot in the weak coupling regime. This allows us to extract the tunnel coupling t as a function of the center gate voltage V_{CG}. In practice, we use a lock-in amplifier technique with a modulation amplitude of 150 μV (applied to LPG) and a frequency of 77.54 Hz to measure the transconductance $\mathrm{dI_{QPC}/dV_{LPG}}$ as a function of detuning δ. This curve consists of the signal we intend to extract superimposed on a slowly varying background originating from the direct cross-talk of the left plunger gate and the QPC. We analyze the data by first subtracting this background, then performing a numerical integration of the data and finally renormalizing the step-height of the resulting signal to one. Three traces of the resulting data are shown in Fig. 3a for different values of t. The tunnel couplings t extracted from this analysis are shown in Fig. 4a together with their 95% confidence intervals.

We also have measured the amplitude and phase of the transmitted signal through the resonator as a function of the dot parameters. We record those signals in the LPG-RPG gate voltage subspace along the δ axis in the vicinity of the charge degeneracy line, see Fig. 3b. Depending on the ratio $2t/h\nu_0$, the resulting traces strongly differ in their phase response as already shown in Ref. 17. In particular, when the qubit frequency $\nu_q = \sqrt{\delta^2 + (2t)^2}/h$ is higher than the resonator eigenfrequency, changing the detuning along the line δ shown in Fig. 2b from a negative value to a positive value shows a reduction of the phase around zero detuning. On the other hand, when the minimum qubit frequency $2t/h$ is lower than the bare resonator frequency ν_0, negative, then positive and again negative phase shifts occur. These phase shifts have been explained in terms of dispersive interaction between the qubit and the resonator [17]. However, probing at a single frequency the amplitude and phase of the transmitted tone does not allow us to unambiguously distinguish between dispersive and dissipative effects. To do so, we acquire an entire frequency spectrum at each point along the detuning line δ. The spectra are fitted with a Lorentzian line shape reproducing the squared amplitude of the transmitted signal

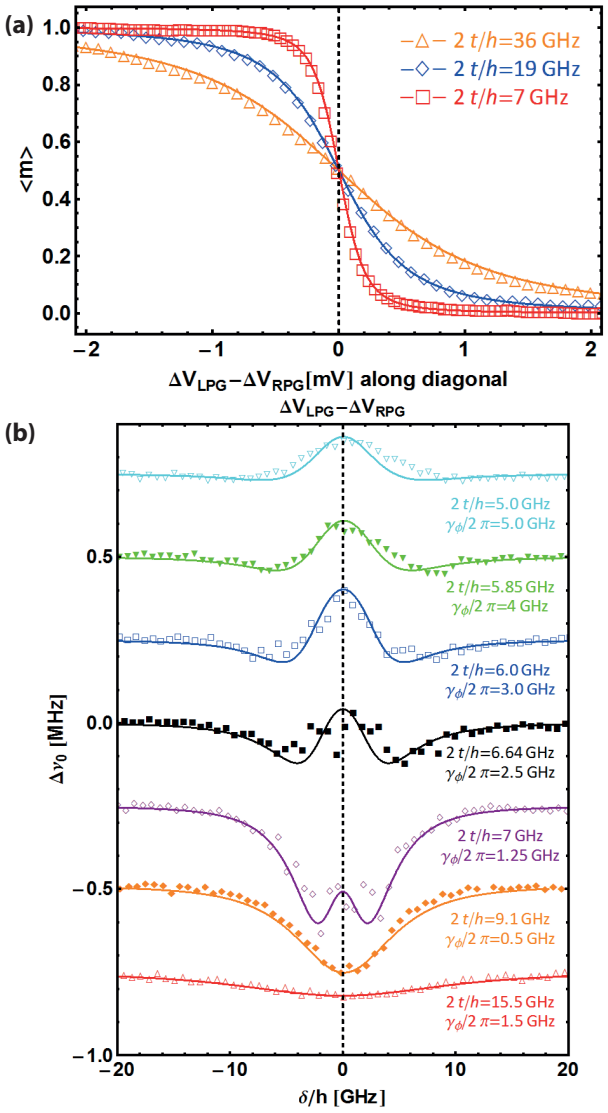

FIG. 3: (a) dc readout: occupation probabilities of the left dot experimentally obtained from a QPC measurement when the voltage $\Delta V_{LPG} - \Delta V_{RPG}$ is swept along the detuning line δ shown in Fig. 2b. The voltage V_{CG} allows to tune the tunnel coupling t between the dots.(b) Microwave readout: frequency shifts (extracted from resonance spectra fits) shown by the resonator along the detuning line δ for different tunneling rates $2t/h$ between the dots.

$A^2 = A_0'^2/(1 + \frac{(\nu-\nu_0')^2}{\delta\nu_0'^2})$. From these fits we extract the resonator frequency shifts $\Delta\nu = \nu_0' - \nu_0$ and the linewidth of the resonator $\kappa'/2\pi = 2\delta\nu_0' = \nu_0'/Q'$ with Q' the modified loaded quality factor of the resonator. We further subtract a slowly varying background in the $\Delta\nu$ response originating from the interaction between the 2DEG and the part of the left plunger gate LPG which traverses the 2DEG separating the resonator from the double dot (independent of dot occupancy). These data are shown in Fig. 3b along the detuning line δ/h expressed in MHz for different values of V_{CG}, i.e. for different tunnel coupling strengths. The conversion of the applied plunger gate voltage to frequency follows from the lever arm consistently extracted from finite bias triangles [2] and electronic temperature broadening of the charge detection linewidth [29].

Our data analysis is based on the simulations described in Ref. 17. In this approach the double quantum dot is modeled as a two-level system which is dipole coupled to a superconducting resonator. This interaction is captured by a Jaynes-Cummings-type Hamiltonian with coupling energy g between the resonator and the qubit, detuning accross the charge degeneracy line δ, tunnel coupling t between the dots and resonator eigenfrequency ν_0 [10]. In order to take into account relaxation γ_1 and dephasing γ_ϕ of the qubit together with the decay rate of the cavity κ we use a Lindblad master equation [17]. In this way we compute the response of the resonator and compare it with the experimental data. We find that all simulations are in reasonable agreement with the data (full lines in Fig. 3b) using the measured values ν_0, κ, estimating a coupling $g/2\pi = 25$ MHz accounting for the differential lever arm of the resonator gate on the two dots, a relaxation rate of the qubit at $\delta \gg t$, $\gamma_1/2\pi = 100$ MHz typical for charge qubits [25] and adjusting tunnel coupling t and dephasing rates $\gamma_\phi/2\pi$ to realize a good fit (see Fig. 3b). The dephasing rates extracted in this way range from 0.5 to 6 GHz and are similar to the ones observed in the experiment by Frey *et al.* which was performed in the many-electron regime [17]. This is surprising, since the excited states spectrum in the single electron regime is expected to be less dense making the qubit less susceptible to energy fluctuations and thus more coherent.

To check for consistency we have repeated the same experiment, with the same sample, in the many-electron regime (≈ 50 electrons in each dot). An increase of the dephasing rates by roughly a factor of two compared to the single-electron regime was observed. This factor of two might be explained considering the lateral extent of the confined wave function of the electrons inside the dots. As the number of electrons increases the wave function extends and turns more sensitive to charge fluctuations occuring in the near vicinity of the dots and voltage fluctuations on the gates. To emphasize this point it is worth noting that the lever arm of the plunger gates increases by a factor of two in the many-electron compared to the single-electron case. Comparing the two situations, a similar gate voltage noise will generate a smaller detuning noise for small lever arms. Accordingly the dephasing rate decreases. However, it is worth noting that given the extracted value of g, the dephasing rate is approximately two orders of magnitude larger than the threshold below which one is expected to be able to observe a vacuum Rabi mode splitting, a prerequisite for circuit QED experiments in the strong coupling regime.

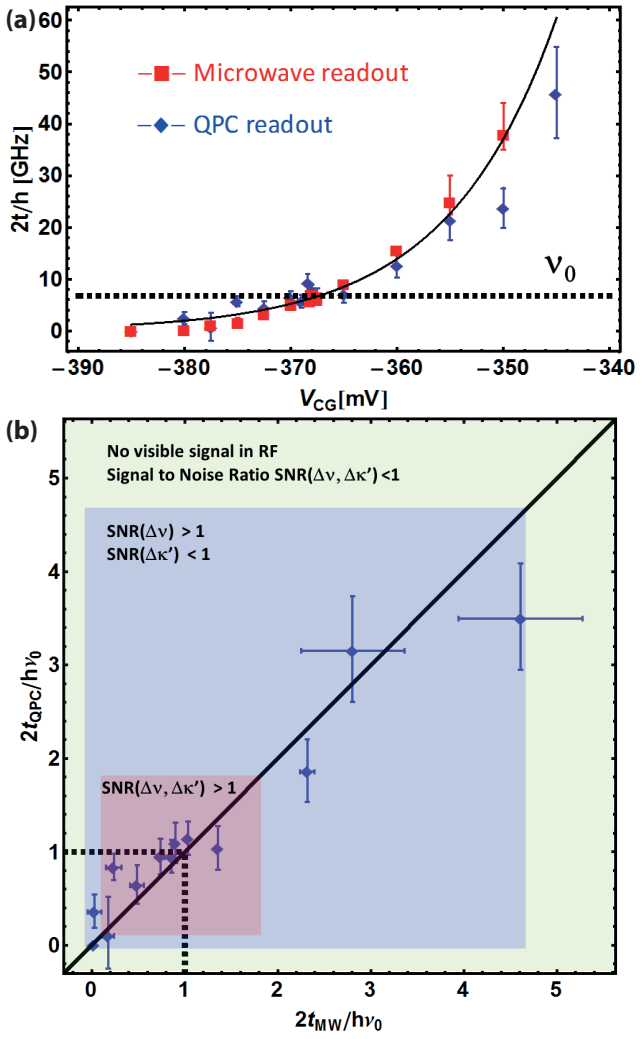

FIG. 4: (a) Tunneling rates $2t/h$ between the dots measured *vs* V_{CG} for the two methods: charge detection with a QPC and microwave polarizability measurement. The black line corresponds to an exponential fit of t *vs* V_{CG}. (b) Comparison of tunnel coupling extracted from dc and microwave measurements. Colored regions highlight the $2t/h\nu_0$ ranges over which $\Delta\nu$ and $\Delta\kappa'$ signals were observable. An observable signal corresponds to a signal to noise ratio $SNR > 1$ when each point of the spectrum are acquired with an integration time $\tau = 168$ ms.

We now discuss the tunnel coupling and its uncertainty extracted from QPC and microwave measurements as a function of $V_{\rm CG}$, see Fig. 4a. For each point, we evaluate the 95% confidence interval of t. For the QPC fits, the evaluation takes into account both statistical errors introduced by the fitting procedure and systematic errors involving uncertainties on the lever arm and in the background subtraction. For the microwave analysis, given that we are unable to use a conventional fitting procedure, we calculate the mean square deviation $Q(t) = 1/N \sum_i [d_i - f_i(t')]^2$ of our data d_i with respect to the calculated data $f_i(t')$ for a number of values of tunneling t'. This mean square deviation can be approximated by a parabolic dispersion $Q(t) = Q_{\rm min} + a(t-t_0)^2$ with a minimum $Q_{\rm min}$ at the value of tunneling t_0 that best reproduces our data and a that parametrizes the dispersion of the deviation when varying t. Whenever $Q(t) = Q_{\rm min}(1 + 4/N)$ one determines the 95% confidence interval $\pm\Delta t$ for t_0. We stress that in this analysis g and γ_1 are fixed and t and γ_ϕ are assumed to be uncorrelated.

From this study, we conclude that there is an overall agreement between the two independent measurement techniques and that the tunneling follows the expected exponential increase with increasing $V_{\rm CG}$ as indicated by the black line in Fig. 4a. Moreover, we find that the analysis of the microwave data allows for a more precise determination of the tunneling amplitude than the charge detection analysis, especially when $2t/h\nu_0 \approx 1$. As an example, we note that for $V_{\rm CG} = -367.5$ mV, tunneling determination with microwaves gives $2t_{\rm MW}/h = 6650 \pm 70$ MHz whereas one obtains $2t_{\rm QPC}/h = 6600 \pm 1500$ MHz in dc. The reason for the higher precision of the microwave analysis stems from the fact that close to resonance the frequency shift changes signs with $1/\Delta$, where Δ is the detuning between the resonator and the DQD.

We also plot the dc *vs* microwave tunnel coupling normalized to the resonator eigenfrequency ν_0 extracted from the experiment in Fig. 4b. This allows us to check the overall consistency of the two measurements and highlight the domains where the microwave detection is sensitive to the DQD polarizability. In particular, it was observed throughout all our measurements that the regions of sensitivity in linewidth $\Delta\kappa'$ and in frequency shifts $\Delta\nu$ to dot polarizability differ in size. A large region exists where only the frequency shift has a signal-to-noise level larger than one for the given integration time of 168 ms, whereas the linewidth broadening is not detectable (blue shaded region in Fig. 4b). This region turns out to be much larger than the one where both frequency shift and linewidth broadening are observed (red shaded region in Fig. 4b).

In summary, we have realized a hybrid device in which we have observed the dipole coupling of a single-electron double quantum dot charge qubit to a superconducting resonator. In order to reach this limit, a quantum point contact was used to probe the charge state of the dot. Comparing the many-electron to the single-electron regime, we did not find significant improvements of the decoherence properties of our double dot system. We further compared two different approaches to determine the tunnel coupling between the dots based on the charge detection using a QPC, and on a charge polarizability measurement of the double quantum dot. The two techniques were found to be equivalent with a superior precision for the polarizability measurement.

We acknowledge fruitful discussions with Clemens Rössler, Jonas Mlynek as well as help with numerical calculations and critical reading of the manuscript from Alexandre Blais. This work was financially supported by EU IP SOLID, by the Swiss National Science Foundation through the National Center of Competence in Research Quantum Science and Technology, and by ETH Zurich.

[1] D. Loss and D.P. DiVincenzo, Phys. Rev. A **57**, 120126 (1998).
[2] W. G. van der Wiel *et al.*, Rev. Mod. Phys. **75**, 1 (2002).
[3] A. Wallraff *et al.*, Nature (London) **431**, 162 (2004).
[4] J. R. Petta *et al.*, Science **309**, 2180 (2005).
[5] R. Hanson *et al.*, Rev. Mod. Phys. **79**, 1217 (2007).
[6] J. Majer *et al.*, Nature (London) **449**, 443 (2007).
[7] R. J. Schoelkopf and S. M. Girvin, Nature (London) **451**, 664 (2008).
[8] T. Obata *et al.*, Phys. Rev. B **81**, 085317 (2010).
[9] T. Ihn, Semiconductor nanostructures, Oxford University Press (2010).
[10] L.Childress, A.S. Sorensen and M.D. Lukin, Phys. Rev. A 69, 042302 (2004).
[11] M. Trif, V. N. Golovach, and D. Loss, Phys. Rev. B **77**, 045434 (2008).
[12] A. Cottet, and T. Kontos, Phys. Rev. Lett. **105**, 160502 (2010).
[13] X. Hu, Y.X. Liu, and F. Nori, Phys. Rev. B **86**, 035314 (2012).
[14] P.Q. Jin *et al.* Phys. Rev. Lett. **108**, 190506 (2012).
[15] N. Lambert, C. Flindt, and Franco Nori, arXiv:1303.7449 (2013).
[16] M. R. Delbecq *et al.*, Phys. Rev. Lett. **107**, 256804 (2011).
[17] T. Frey *et al.*, Phys. Rev. Lett. **108**, 046807 (2012).
[18] T. Frey *et al.*, Phys. Rev. B **86**, 115303 (2012).
[19] K. D. Petersson *et al.*, Nature **490**, 380 (2012).
[20] H. Toida, T. Nakajima, and S. Komiyama, Phys. Rev. Lett. **110**, 066802 (2013).
[21] M. R. Delbecq *et al.*, Nat. Commun. **4** 1400 (2013).
[22] T. Frey *et al.*, Applied Physics Letters **98**, 262105 (2011).
[23] J. Raimond, M. Brune, and S. Haroche, Rev. Mod. Phys. **73**, 565582 (2001).
[24] J.M. Elzerman *et al.*, Nature **430**, 431 (2004).
[25] J. R. Petta *et al.*, Phys. Rev. Lett. **93**, 186802 (2004).
[26] M. Pioro-Ladrière *et al.*, Nature Physics **4**, 776 (2008).
[27] M. Field *et al.*, Phys. Rev. Lett. **70**, 1311 (1993).
[28] J.M. Elzerman *et al.*, Phys. Rev. B **67**, 161308(R) (2003).
[29] L. Di Carlo *et al.*, Phys. Rev. Lett. **92**, 226801 (2004).